Modeling breakup and relaxation of Newtonian droplets using the advected phase-field approach

J. Beaucourt, T. Biben, A. Leyrat, and C. Verdier*
Laboratoire de Spectrométrie Physique, Université Joseph Fourier Grenoble I and CNRS (UMR5588), 140 avenue de la physique, Boîte Postale 87, 38402 Saint Martin d'Hères cedex, France
(Received 5 January 2006; revised manuscript received 3 November 2006; published 23 February 2007)

The relaxation and breakup of Newtonian droplets is considered using the advected field approach. This method allows one to follow the deformation of interfaces using an order parameter field [Biben *et al.*, Europhys. Lett. **63**, 623 (2003)] based on a Ginzburg-Landau equation. Using this method, it is possible to follow the breakup of droplets and stability curves can be obtained in both two- and three-dimensional shear and elongational flows. Finally, relaxation of a droplet is considered, following the application of an elongational flow. The results are compared with previous experimental data [Ha and Leal, Phys. Fluids **13**, 1568 (2001)], and are found to be in satisfactory agreement. The method is general enough to be applied to other non-Newtonian fluids, such as Oldroyd-B fluids or viscoplastic materials.

DOI: 10.1103/PhysRevE.75.021405 PACS number(s): 47.55.D−, 47.20.Dr, 82.70.Kj, 47.55.df

INTRODUCTION

The droplet breakup problem was introduced long ago by Taylor [1,2] both experimentally and theoretically. Using roller devices, he was able to produce two-dimensional shear and elongational flows and applied them to investigate viscous droplet deformation in a viscous suspending fluid. Such flows can lead to stable droplet deformation or to droplet breakup. If η_1 is the droplet viscosity, η_2 the suspending fluid viscosity, $\dot{\gamma}$ the rate of deformation in shear or elongation, and σ the interfacial tension, two dimensionless control parameters can be constructed to determine droplet dynamics. The first one is the capillary number $\mathrm{Ca}=\eta_2 R\dot{\gamma}/\sigma$, and the second is the viscosity ratio $\lambda=\eta_1/\eta_2$.

Following this approach, Grace [3] demonstrated experimentally that critical deformations and capillary numbers for breakup can be determined as functions of λ in shear and elongational flows, over ten decades. This was also investigated in the case of mixed flows [4]. Results from Grace [3] show that it is easier to break droplets in elongation than in shear. A shear flow is indeed the combination of an elongation along the diagonal axes, at 45° from the shear direction, and a rotation tilting the drop. The competition between these two components is controlled by the viscosity ratio; in particular, a droplet cannot be broken in a shear flow [3] when the viscosity ratio λ is larger than roughly 3.5. At large viscosity ratios, the rotational component of the flow tends to orient the main axis of the drop along the shear direction, where elongational effects are weak.

The shape of the droplets in such flows is also a point of interest. Torza *et al.* [5] have shown that droplet shapes can vary quite a lot with the viscosity ratio λ, in particular small ratios lead to droplets with pointed ends. The prediction of droplet deformation has been considered from a theoretical as well as a numerical point of view. Analytical models based on small deformation theory [6], slender body theory [7,8], or using matched asymptotics [9] have been developed, allowing predictions of the critical capillary number for droplet breakup, also named the onset of "burst." In particular, using perturbations of the flow around the droplet, stability analysis leads to a surprisingly good prediction of the critical capillary number [6], as a function of the viscosity ratio λ. With the development of numerical methods such as the boundary integral method [10–14], calculations have also made considerable advances, allowing for more intricate shapes to be obtained accurately. This is of utmost importance when looking at nonlinear effects, as exhibited when stretching filaments or breaking drops into two or more droplets, or forming satellite droplets [2,15].

The numerical technique should not only allow one to predict the burst criterion (in a possible large range of viscosity ratios) but should also give the exact details of the droplet rupture sequence, such as the rupture time, the shape of the filament at pinchoff [15–19], the number of droplets, and their size [3,19]. In particular, close attention needs to be paid to the physics involved in the rupture process, in order to determine whether it is initiated by capillary waves [15] or if it has a deterministic nature, in relation to the well-defined Rayleigh instability [20,21].

Along with the boundary integral methods, new techniques appeared such as the level set [19,22–24], the volume-of-fluid method [25], and the phase-field approach [26–31], which allow computation of two- and three-dimensional flows, for various deformable entities under flow, such as droplets or vesicles. The advantage of these new methods relies on their ability to deal with various constitutive equations for the inner or outer fluid (Oldroyd-B fluid [24], yield-stress fluid [32]). Also, such problems can be solved in the whole domain, without having to consider explicitly the moving interfaces. The complexity of the particle can also be investigated; in particular one may study drops with compatibilizers [33,34], capsules [35], or vesicles [26]. Finally, the ability of such a technique to predict breakup (and coalescence) seems promising for the understanding of multiphase flows [29,30], and the rheology of emulsions, which have been problems of interest for many years [1,36–38].

In this paper, we propose to test the ability of the advected phase-field approach [27] to investigate the dynamics of

*Author to whom correspondence should be addressed. FAX: +33 4 76 63 54 95. Electronic address: verdier@ujf-grenoble.fr

droplet breakup and relaxation. The main motivation is to compute stability curves as depicted by Grace [3], but also to follow the relaxation of droplets following a step-up in elongation, as studied previously [12,39,40]. Numerical simulations will then be compared with previous studies, including experimental results.

In Sec. I, the model is presented. Then finite-size effects are discussed (Sec. II) in the case of relaxation of a long drop, with no applied flow. Indeed, confinement can affect the dynamics of drop relaxation. Stability curves are exhibited and compared with experimental data and previous computations (Sec. III). In Sec. IV, we focus on droplet relaxation, following the paper of Ha and Leal [40], where extensive data are reported on the effect of the initial stretch on droplet relaxation. Comparisons between numerical data and experiments are discussed.

I. THE ADVECTED FIELD METHOD

The main idea inherent in this method is to consider a fluid-fluid interface as a diffuse locus where a function ϕ (phase field) goes smoothly from -1 to $+1$. In this case, -1 designates one fluid and $+1$ the other fluid component. This method is well adapted for describing binary fluids, in particular immiscible fluids. ϕ varies with time t and position $\mathbf{r}$ and may be regarded as a rescaled concentration, as in diffusion problems.

For the study of such binary systems, one can use the following free-energy functional $F[\phi]$, a functional of $\phi(\mathbf{r},t)$ [41]:

$$F[\phi] = \int_V \left(W(\phi) + \frac{\epsilon^2}{2}|\nabla\phi|^2 \right) dV \tag{1}$$

where $W(\phi)$ is the thermodynamic potential

$$W(\phi) = \frac{1}{4}(1-\phi^2)^2. \tag{2}$$

This determines the two equilibrium values ± 1, and the shape across a planar interface at equilibrium, which is simply given by $\phi(r)=\tanh(r/\epsilon\sqrt{2})$. The interface thickness is thus $\epsilon\sqrt{2}$. The temporal evolution equation for the field ϕ shows the competition between the relaxation to the equilibrium profile, described here using an Allen-Cahn approach [42,43], and the advection due to the flow field

$$\frac{\partial\phi}{\partial t} + \mathbf{v}\cdot\nabla\phi = -\Gamma\left(\frac{dW}{d\phi} - \epsilon^2\Delta\phi\right) \tag{3}$$

where $\mathbf{v}$ is the velocity field, and $1/\Gamma$ is the Allen-Cahn relaxation time. A conservative version of this equation can be obtained by replacing the constant Γ by $-\Gamma\Delta$, Γ being in this case a diffusion constant and Δ the Laplacian operator (Cahn-Hilliard prescription). Although this kind of theory has been used for the description of thermocapillary flows [44], it cannot describe the dynamics of mesoscopic droplets accurately. The main reason is due to the value of ϵ, the interfacial thickness, which should be around a 1 nm. For a 10 μm droplet (radius R), $\epsilon \simeq 10^{-4}R$ is out of reach: in practice we use $0.04R$ instead. Overestimation of ϵ has an important consequence: the interfacial tension $\epsilon\int_{-1}^{+1}\sqrt{2W(\phi)}d\phi$ [41], which is implicitly contained in the Allen-Cahn approach, is too large, and is not coupled with the velocity field in this approach. A drop will thus relax to equilibrium (spherical shape) even in the absence of flow when the dynamics is conserved, whereas it will vanish if the dynamics is not. As described earlier [26,27,45], we propose to add a counterterm, which cancels the effect due to the Allen-Cahn surface tension, in order to avoid this problem. The true surface tension σ is accounted for in the velocity field dynamics. It is important to note that this counterterm improves the stability of satellite droplets in a very efficient way, otherwise they would simply disappear in a standard Allen-Cahn formulation. We shall see examples of this fact below. The new formulation is

$$\frac{\partial\phi}{\partial t} + \mathbf{v}\cdot\nabla\phi = -\Gamma\left\{\frac{dW}{d\phi} - \epsilon^2(\Delta\phi + c|\nabla\phi|)\right\}. \tag{4}$$

In this new equation, c is the local curvature. This expression can be derived from an asymptotic expansion, corresponding to the limit $\epsilon \to 0$. The counterterm simply cancels the first-order correction in ϵ, and thus extends the validity of the theory to larger values of ϵ. At this order, it replaces the Laplacian of ϕ by $\partial^2\phi/\partial r^2$, the second-order derivative in the normal direction only. The equilibrium shape of the interface is still given by

$$\phi(r) = \tanh(r/\epsilon\sqrt{2}) \tag{5}$$

but this is now valid whatever the curvature of the interface, because only the radial (normal) component r measured across the area is relevant here.

Due to the presence of the restoring term on the right-hand side of (4), the field ϕ now becomes a passive variable whose value is prescribed by the hyperbolic tangent formula. $\phi=0$ corresponds to the real interface locus.

Finally, the velocity field is the solution of the momentum equation:

$$\rho\left(\frac{\partial\mathbf{v}}{\partial t} + \mathbf{v}\cdot\nabla\mathbf{v}\right) = -\nabla p + \nabla\cdot\boldsymbol{\Sigma} + \mathbf{F}_{int} \tag{6}$$

where ρ is the common density of both fluids, $\mathbf{v}$ the macroscopic velocity field, $\boldsymbol{\Sigma}$ the stress tensor, and $\mathbf{F}_{int}$ the force due to interfacial tension, which is located at the interface and has been added to the momentum balance. In fact, $\mathbf{F}_{int}$ is simply given by

$$\mathbf{F}_{int} = \frac{c}{2}\sigma\nabla\phi. \tag{7}$$

The shape function of the interface $\delta(r)$ can be defined by $\nabla\phi/2 \equiv \delta(r)\mathbf{n}$, where $\mathbf{n}$ is a unit normal vector to the interface pointed outward, $\delta(r)$ becoming a Dirac distribution in the sharp interface limit. Note that the curvature is defined by $c=-\nabla\cdot\mathbf{n}$ (negative for a sphere). The stress field $\boldsymbol{\Sigma}$ is given by Newton's law, $\boldsymbol{\Sigma}=2\eta(\phi)\mathbf{D}$, where $\mathbf{D}$ is the symmetric part of the velocity gradient tensor $\nabla\mathbf{v}$. The viscosity $\eta(\phi)$ is

domain dependent and the system of equations (4), (6), (7) may be solved together with the incompressibility condition

$$\nabla \cdot \mathbf{v} = 0. \tag{8}$$

The boundary conditions and initial conditions will be specified below. Note that the viscosity is allowed to vary smoothly across the interface by prescribing it to be

$$\eta(\phi) = \frac{1}{2}\{\eta_1(1-\phi) + \eta_2(1+\phi)\}. \tag{9}$$

The value corresponding to the location of the interface ($\phi=0$) is simply the average $(\eta_1+\eta_2)/2$. Note that, when using (6), care needs to be taken of the derivative of the viscosity, which is no longer a constant. The method can also allow for density contrasts, but this will not be studied here. Inertia is controlled by the Reynolds number $\mathrm{Re}=\rho R^2\dot{\gamma}/\eta_2$, when a deformation rate $\dot{\gamma}$ is applied, and conversely by a Suratman number $\mathrm{Su}=\rho R\sigma/\eta_2^2$, when relaxation phenomena are considered. In this last situation, the velocity scale is indeed a result of the capillary relaxation: the surface-tension-induced velocity is σ/η_2. In the case of interest, these two dimensionless parameters (Re and Su) are quite small, as in Stokes flow.

The method used is based on the calculation of ϕ, the pressure p, and the velocity field $\mathbf{v}$. ϕ is found using a finite difference scheme [Eq. (4)], whereas the velocity field is obtained from (6) in the Fourier space. For this purpose, we use a regular rectangular grid, with cubic [three dimensional (3D)] or square elements (2D or 3D axisymmetric). The spacing is chosen to be exactly ϵ, where $\epsilon=0.04R$. The flow field $\mathbf{v}$ can be divided into two components; the undisturbed external flow field $\mathbf{v}_{ext}$ (shear or elongational flow), and a contribution $\mathbf{u}$, which is due to the flow induced by the droplet. The boundary conditions are chosen to be periodic for the advected field ϕ, and also for $\mathbf{u}=\mathbf{v}-\mathbf{v}_{ext}$.

This enables us to solve for relatively small droplets, but satellite droplets smaller than ϵ are obviously not visible. In such cases, other more technical methods may be relevant such as the ones used in solidification problems, like the boundary element method of Almgren [46] or the phase-field model by Wheeler and coauthors [47].

II. FINITE SIZE EFFECTS

It is important to analyze the strong influence of finite size effects on the breakup sequence, for example when following the relaxation of a drop in a quiescent fluid. To discuss this point in more detail, we specify the geometry and the values of the resolution parameters such as the grid spacing and its size. Since we considered 2D and 3D axisymmetric situations, the resolution box is a rectangle of size $N_x h \times N_y h$, where h is the lattice spacing (square elements). In 2D, x and y denote the usual coordinates, while in a 3D axisymmetric geometry, x corresponds to the coordinate along the axis and y the radial coordinate. A droplet is initially placed at the center of the grid. Since we make extensive use of Fourier Transformations, we still consider the full grid for 3D axisymmetric situations, while a direct space implementation could reduce the problem to a quarter of the grid only, accounting for the symmetries. The boundary conditions on the velocity field are chosen to reduce the boundary effects: we considered periodic boundary conditions for the counter flow induced by the drop, as specified in Sec. I. We fixed $h=0.04R$ in order to have a sufficient resolution to describe the rapid variation of the advected field across the interface, and to have a small enough value of ϵ, the phase-field width. All results reported in Secs. III and IV have been obtained with $N_x=1200$ and $N_y=800$, corresponding to a typical box size $48R\times 32R$ in units of the drop radius. We also considered a smaller box $N_x=800$ and $N_y=200$ ($32R\times 8R$) that were shown to be too small to provide robust data.

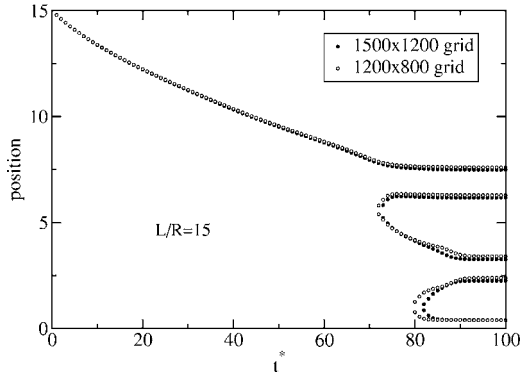

FIG. 1. Dimensionless position of fragment edges as a function of the reduced time $t^*=t\sigma/\eta_2 R$ (i.e., trajectories). $L/R=15$. Two different box sizes give rise to similar scenarios.

We investigated the simple case of a spherocylindrical drop of initial half-length $L/R=15$ (L the half-length R the radius of the equivalent spherical drop) to determine the influence of finite size effects. We varied N_x and N_y in a large range: $800\leq N_x\leq 1500$ and $200\leq N_y\leq 1500$. We also tested the breakup sequence for $L/R=18$ and a 1500×1500 grid. We consider that two fragmentation sequences are equivalent when small quantitative differences are observed, as shown in Fig. 1.

In Table I, results obtained for $L/R=15$ are summarized. A full line separating two different box sizes indicates differ-

TABLE I. Summary of the data obtained for relaxation of a spherocylindrical drop with an initial half-length $L/R=15$. The straight solid lines separate regions with very different fragmentation sequences while dashed lines correspond to apparent differences only.

1500x1500	1200x1500		
1500x1200	1200x1200	1000x1200	800x1200
	1200x1000	1000x1000	800x1000
	1200x800	1000x800	800x800
		1000x600	800x600
	1200x400	1000x400	800x400
	1200x200	1000x200	800x200

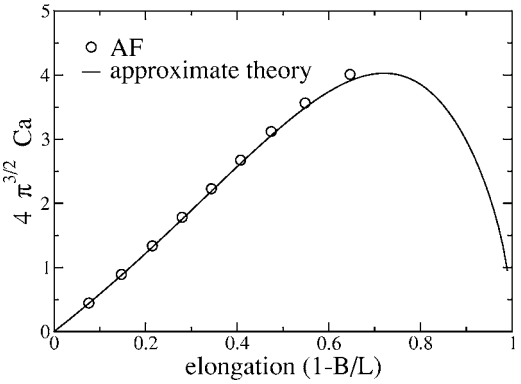

FIG. 2. Capillary number vs elongation parameter $1-B/L$ ($\lambda=1$) [48].

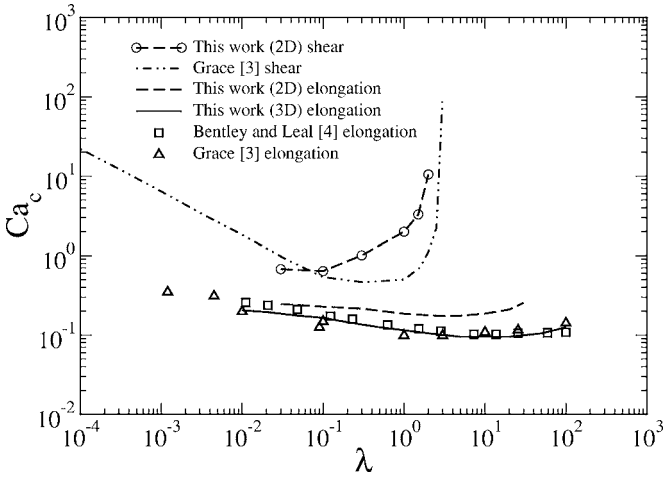

FIG. 3. Critical capillary number Ca_c vs viscosity ratio λ in 2D and 3D shear and elongational flows.

ent fragmentation sequences. The dashed line corresponds to equivalent results, but due to the proximity of a transition between five fragments ($L/R=15$) and seven fragments ($L/R=15.1$) for a 1200×800 grid, a slight difference is observed in the fragmentation sequence. Consequently, we also explored neighboring values of L/R to check this feature. From Table I, 1200×800 seems to be a good compromise between accuracy and computational speed. Therefore, in what follows, we will use such a mesh corresponding to a box size $48R\times32R$.

III. STABILITY CURVES

We first investigate the ability of the method to predict deformation and breakup of drops accurately. In order to do so, we consider Buckmaster and Flaherty's analytical solution [48] of the flow around a droplet in a 2D elongational applied flow. This flow corresponds to $v^x_{ext}=\dot{\gamma}x$, $v^y_{ext}=-\dot{\gamma}y$, where x is the coordinate along the axis of the drop. The authors [48] were able to calculate the deformation of the drop up to the burst transition. Results of our simulations are presented in Fig. 2 and compared with their approximate theory. Below a critical capillary number Ca_c, the drop deforms until it reaches a steady shape [3] that can be characterized by its elongation $1-B/L$, where B is the half-width, and L is the half-length. B/L being always smaller than 1, the drop has a prolate shape. Above Ca_c, the drop is elongated until it breaks. Such a behavior corresponds to a saddle node bifurcation; thus an unstable branch exists which merges with a stable one at a critical capillary number. While the stable branch corresponds to convex shapes, the unstable one accounts for non-convex shapes. The critical capillary number is determined by the maximum of the curve in Fig. 2, giving approximately $Ca_c\simeq0.18$, according to their results. Figure 2 also shows a good comparison between the theory [48] and results obtained with the present advected field (AF) method for $\lambda=1$. The predictions of the AF method are quite accurate.

The case of a drop subjected to a shear flow or an elongational flow is considered next. The results are shown in Fig. 3. Numerical data have been obtained for two particular geometries: a 2D geometry for both the droplet and the applied flow (shear or elongation), and a 3D axisymmetric geometry for an applied elongational flow. In the 2D situation, the shear flow is defined by $v^x_{ext}=\dot{\gamma}y$, $v^y_{ext}=0$, and the elongational flow by $v^x_{ext}=\dot{\gamma}x$, $v^y_{ext}=-\dot{\gamma}y$. The 3D axisymmetric elongational flow corresponds to $v^x_{ext}=\dot{\gamma}x$, $v^r_{ext}=-\dot{\gamma}r/2$, in cylindrical coordinates, where x is the direction of elongation and r is the radial coordinate. A comparison between the numerical data and the experiments reported in [3] is difficult since the experimental geometry is a combination of 2D features, like the applied flow in shearing and elongation experiments using the four-roll apparatus [4], and 3D features associated with droplet deformation. It is interesting to note the overall qualitative agreement between the numerical data and the experimental one. For example, in the 2D shear situation, there is a stable region at viscosity ratios above $\lambda=4$ roughly, as in 3D. Finally, the 3D axisymmetric elongation data compare very well with the four-roll apparatus experiments [3,4]. Quantitative discrepancies are, however, observed when comparing 2D data to experiments, in particular in shearing flows. This shows that 2D models, although not fully quantitative, can be helpful for the study of multiphase flows. Furthermore, the excellent agreement in 3D demonstrates the ability of the AF formulation to capture the physics involved in the burst transition, at least for the viscosity ratios we considered.

Our study was limited to viscosity ratios between 0.01 and 100. This is already a very satisfactory result, covering four decades in λ. When small viscosity ratios are considered (say $\lambda<0.01$), droplets exhibit pointed ends, and the method fails to predict such shapes because it is unable to account for large curvatures. Indeed, the small radius of curvature at the ends becomes close to the size of the mesh ϵ, therefore the method cannot give accurate solutions. This AF method is also in agreement with the small deformation theory [6], which predicts well the data in this region, as pointed out by the authors in previous work [27]. Our data are not exhaustive, in particular 3D simulations of shear flows are not provided due to the long times involved for carrying out such computations. Some of these data is available in another paper [25].

IV. DROPLET RELAXATION

The relaxation of droplets following an elongation is an interesting problem, since it raises the questions of the number of fragments, and the relaxation of the drop to its initial state or not. It has been explored both experimentally [39,40,49–51] and numerically [12,50,51]. It is well known that the initial deformation controls the fate of the relaxing droplet. The initial length L is an obvious control parameter, but parameters like the capillary number Ca and the viscosity ratio λ are also of importance. Recently, Ha and Leal [40] considered the problem of droplet relaxation following a step-up in elongation, using their four-roll mill apparatus. At low Reynolds numbers, when the capillary number is larger than its critical value for breakup, they showed that the critical stretch ratio L/R for breakup increases sharply with the capillary number. An interesting feature also occurs, which is the restabilization of the droplet when increasing the initial stretch ratio at a fixed capillary number. The droplet relaxes first to a sphere at small initial stretch ratio, then into two droplets (first transition), then relaxes into a sphere again, and finally into three droplets (second transition). This feature was observed at a viscosity ratio $\lambda=0.056$ and for $\mathrm{Ca}/\mathrm{Ca}_c=2.15$ [40]. Therefore, more investigations remain to be done in order to see whether this feature is always present, and if such a cascade of restabilizations is possible.

This type of approach is now conducted, in a 3D axisymmetric situation.

Before discussing the results in details, we shall first identify the parameters entering in this problem. The elongation-relaxation experiments are essentially controlled by three parameters: the capillary number Ca (or alternatively $\mathrm{Ca}/\mathrm{Ca}_c$), the stretch ratio L/R, which corresponds to the maximal elongation of the drop, and the viscosity ratio λ. Whereas these three parameters play a role during the elongation stage, and determine the shape of the drop after relaxation, only λ plays a role during the relaxation stage (for a given initial shape). Indeed the capillary number is not defined (no applied flow), and the capillary time can be absorbed by a redefinition of the time scales $t^*=t\sigma/\eta_2 R$, where t^* is the dimensionless time. We shall thus mainly focus on $\mathrm{Ca}/\mathrm{Ca}_c$ and L/R to control the initial shape of the relaxing drop, and the particular role of λ will be briefly discussed.

A. Comparison with experiments

Here we consider the experimental situation of Ha and Leal where the drop is elongated until it reaches a given stretch ratio, and follows a free relaxation afterwards. A first set of data is obtained for $\mathrm{Ca}/\mathrm{Ca}_c=1.05$, and a viscosity ratio $\lambda=0.2$. These values are very similar to those used by Ha and Leal (they used $\lambda=0.209$ and found $\mathrm{Ca}_c=0.135$, whereas here $\lambda=0.2$ and $\mathrm{Ca}_c=0.151$). The results are presented in Fig. 4, showing the effect of a change in the stretch ratio L/R. This enables to determine a critical stretch ratio $(L/R)_c$ above which the drop starts to break during the relaxation stage. Figure 4 shows the variation of the drop elongation with time. The instantaneous stretch ratio $L(t)/R$ should not be confused with the maximum stretch ratio L/R. The features of the curves $L(t)/R$ are as follows: when L/R is smaller than roughly 3.9, the drop is stretched and relaxes to a spherical shape, whereas if L/R is larger than 3.9, the drop relaxes into two droplets. Note that a satellite droplet is also observed ($L/R=4.2$), with a very small size of the order of a few times the value of ϵ. Attention thus needs to be paid regarding this feature both in simulations and in experiments. Our observations are however in good agreement with the experiments of Ha and Leal.

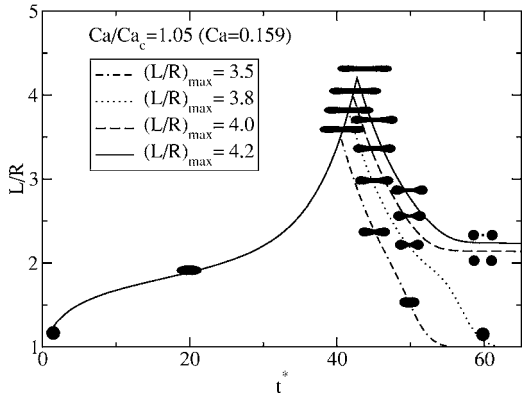

FIG. 4. $\mathrm{Ca}=0.159$. $\mathrm{Ca}_c=0.151$. $\mathrm{Ca}/\mathrm{Ca}_c=1.05$. Relaxation patterns at different values of L/R (3.5,3.8,4.0,4.2) and $\lambda=0.2$. $t^*=t\sigma/\eta_2 R$.

While the previous example corresponds to a capillary number very close to the critical capillary number ($\mathrm{Ca}/\mathrm{Ca}_c=1.05$), it is interesting to consider larger values. We can carry out a similar analysis for $\mathrm{Ca}/\mathrm{Ca}_c=2.11$ (and still $\lambda=0.2$). The results are presented in Table II and show similarities with the previous example (a succession of one, two and three fragments with a satellite central drop while increasing the stretch ratio L/R), but more interesting is the restabilization sequence.

The transition from two to three droplets occurs between $L/R=7.4$ and 7.45. Then a restabilization is observed for $L/R=7.9$ for which two fragments are produced. Again, we find the formation of three fragments at $L/R=8.0$, indicating that the region of restabilization was very small. Whereas Ha and Leal reported a restabilization scenario from two to one

TABLE II. Breakup events for different L/R ($\lambda=0.2$, $\mathrm{Ca}=0.326$, $\mathrm{Ca}/\mathrm{Ca}_c=2.11$). N is the number of fragments.

L/R	N	Comment
6.5	1	
7.0	1	
7.1	1	
7.2	2	
7.4	2	
7.45	3	Satellite central drop
7.8	3	Satellite central drop
7.9	2	No central drop
8.0	3	Small central drop
8.4	3	Small central drop
8.5	5	Alternating large and satellite drops

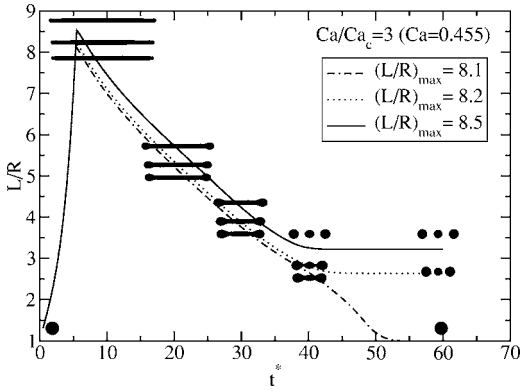

FIG. 5. Ca=0.455. Ca_c=0.151. Ca/Ca_c=3.0. Relaxation patterns at different L/R (8.1,8.2,8.5) and λ=0.2. $t^*=t\sigma/\eta_2 R$.

droplet (at a viscosity ratio of λ=0.056, which we shall consider below), the restabilization situation observed here seems to be different.

It is tempting to increase the capillary number further in order to observe more complex sequences. This is precisely what is done for λ=0.2, Ca/Ca_c=3, as shown in Fig. 5. We find a larger critical value $(L/R)_c$=8.15 in this case, in agreement with the experiments, but the overall fragmentation sequence seems to be simpler than the previous one. We shall, however, mention that we do not observe the fragmentation into two droplets for this set of parameters, instead, the drop relaxes into three droplets, after cessation of flow, above the critical stretch ratio. For this computation, as the capillary number is rather large due to the large elongation rate used (steep increase of L/R in time), the time step in the finite difference scheme has been reduced to avoid instabilities.

These three examples illustrate quite well the complexity of the fragmentation sequences, and the non trivial dependence on the control parameters. We could observe a high sensitivity of the results to the control parameters, in particular the restabilization observed in the second example presented above only exists in a very narrow range of parameters (between L/R=7.9 and 8.0) that could be easily missed experimentally.

To complete the comparison with the experimental work of Ha and Leal, we plot the critical stretch ratios obtained for λ=0.2 in Fig. 6.

These values correspond to the first transition from a sphere to two or more spherical droplets plotted as a function

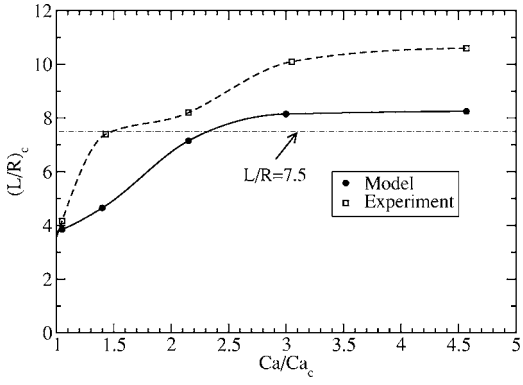

FIG. 6. Critical L/R vs Ca/Ca_c at a viscosity ratio λ=0.2.

of the capillary ratio Ca/Ca_c. The capillary numbers are all higher than the critical one, to be able to obtain droplet breakup. Also shown is the experimental data by Ha and Leal (Fig. 3 of their paper), found to be in qualitative agreement. The discrepancy might be due to the difficulty to control the stretching rate accurately in the experiments. Another explanation may be that a smaller value of ϵ is needed in the simulations for them to become more accurate. This was not possible due to the large systems considered here. Let us finally mention the accuracy of our 2D simulations found previously (Fig. 2) for similar values of ϵ.

B. Influence of the capillary number

In the previous part, we observed that the capillary number plays a complex role in the restabilization process. Our purpose is now to identify this role more precisely. With this aim, we shall consider a fixed stretch ratio L/R=7.5, and investigate the relaxation sequence as a function of the capillary number used to produce the elongated shape. We thus follow the horizontal path plotted in Fig. 6. This value has been chosen to match the data of Ha and Leal (Fig. 2 of Ref. [40]), still at a viscosity ratio of 0.2. Figures 7(a)–7(c) show the different relaxation mechanisms, following stretching rates at capillary numbers of 0.212, 0.326, and 0.455, respectively.

The first breaking pattern leads to the formation of a long elongated droplet in the center, which eventually breaks due to end pinching [15–18], thus forming three droplets. In the second case, larger side droplets are formed and the central resulting droplet is smaller, but they are still three. Finally, as the capillary number is increased again, the initial shape of the droplet is different, exhibiting pointed ends, as expected for such a small viscosity ratio. This feature is due to the fast elongation process, inhibiting the creation of bulbed ends. Thus the elongated droplet relaxes into one final drop.

Whereas the elongated drops present bulbed ends at small capillary numbers, favoring fragmentation in a relaxation experiment, they do not present these features at large capillary numbers. In this case, the bulbed ends responsible for the breakup process must be produced during the relaxation, which can take time. If relaxation is not efficient enough for the drop to develop bulbed ends rapidly, then the droplet relaxes to a sphere.

Large values of Ca/Ca_c thus do not favor the fragmentation, and the most interesting restabilization sequences were observed around Ca/Ca_c=2.11–2.15, at λ=0.2.

C. Restabilization

In this part we investigate the restabilization sequence in more detail. We would like to emphasize that this feature is generic, and can be observed for many values of the parameters. Moreover, we also would like to show that such restabilization sequences are very sensitive to the precise values of the parameters and can present a huge richness. We thus used a set of parameters also considered by Ha and Leal [40] (λ=0.056 and Ca/Ca_c=2.15), and we shall compare results with the previous restabilization sequence (λ=0.2 and Ca/Ca_c=2.11, from Table II).

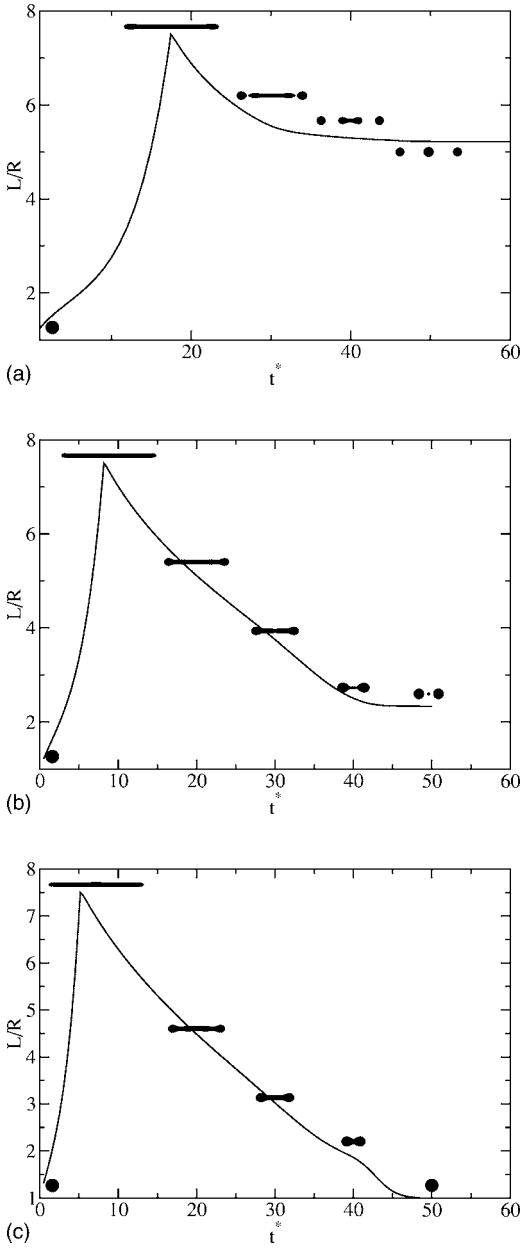

FIG. 7. Relaxation pattern following elongation. Stretch ratio $L/R=7.5$. $\lambda=0.2$. $Ca_c=0.151$. $t^*=t\sigma/\eta_2 R$. (a) $Ca=0.212$, $Ca/Ca_c=1.4$. (b) $Ca=0.326$, $Ca/Ca_c=2.15$. (c) $Ca=0.455$, $Ca/Ca_c=3$.

The observations are shown in Fig. 8, where the droplet has been elongated from its initial spherical shape to a certain state characterized by a value of L/R, at a capillary number $Ca=0.359$. For this case, the critical capillary number is found to be $Ca_c=0.167$ (thus $Ca/Ca_c=2.15$). An interesting series of droplet breakups is observed. This scenario is very similar to the experiments of Ha and Leal: first the droplet is elongated but relaxes to a single sphere $L/R=6.9$; the droplet breaks up into two spheres $L/R=7.1$; the droplet restabilizes and goes back into a sphere $L/R=7.3$; the droplet breaks into three droplets $L/R=7.5$; the central droplets disappears and two droplets are obtained $L/R=7.7$; and finally the central drop is formed again and we end up with three drops $L/R=8.5$

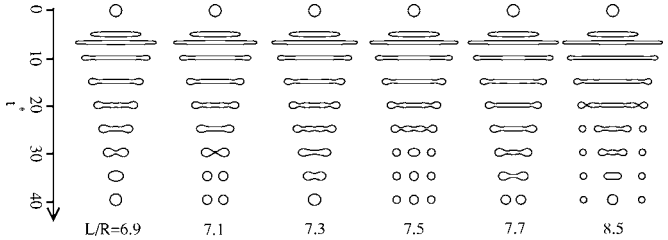

FIG. 8. Relaxation of droplets after stretching at a given L/R ($Ca/Ca_c=2.15$, $\lambda=0.056$, $Ca_c=0.167$). $t^*=t\sigma/\eta_2 R$.

As expected from the work of Ha and Leal [40], these results confirm the idea that the mechanism of relaxation, which is governed by two parameters, λ and the initial shape of the droplet, is based on the following idea. A droplet relaxes by forming first bulbed ends, which need to have enough time to develop [12]. After this deformation is achieved, the droplet motion is governed by the stability of the filament, which can be described accurately by linear stability analysis [12,20]. Following the work of Tomotika [20,21], predictions of the most unstable mode can be obtained when the viscosity ratio λ is known. Of course, this study has been carried out when the outer fluid is at rest, but nevertheless it seems to predict rather well the onset of stability [12]. Analysis of the previous droplet shapes reveals that, after bulbed ends are formed, the length of the filament seems to predict rather well the evolution of the droplet to an unstable situation or not.

Another interesting aspect is the restabilization of the droplet independently of its size, as revealed by the succession of shapes in Fig. 8. From $L/R=7.1$ to 7.3, the droplet restabilizes. From $L/R=7.5$ to 7.7, restabilization is also obtained, but now the central droplet has disappeared. This phenomenon is also observed at different viscosity ratios, and could be universal. Even in this case the restabilization differs from the situation presented in Table II by the fact that the central fragments for $\lambda=0.2$ are small satellite droplets whereas for $\lambda=0.056$ they correspond to the largest fragment.

A case of interest would be to follow systematically the fragmentation process as L/R is increased and for a fixed λ. This should allow one to determine whether fragmentation is governed by a deterministic process or exhibits a chaotic behavior. This still requires improvement of the numerical scheme presented here in terms of precision (i.e., smaller values of ϵ, mesh adaptation, etc.) in order to capture the formation of smaller daughter droplets including satellites. This work is currently under way.

CONCLUSION

We presented a comparison between the elongation-relaxation experimental data obtained by Ha and Leal and the numerical data obtained with the advected field method. Although we observe quantitative differences between 2D shear simulations and 3D experimental data, which can be explained by the difference of dimensionality, the numerical data obtained in 3D are in very good agreement with the

experimental findings. In particular, the method is able to reproduce the complex fragmentation-restabilization sequence observed experimentally, and may give the possibility of investigating simpler drop geometries such as the spherocylindrical shape. The observed behaviors are deterministic, and the restabilization sequences are responsible for the apparent noise in the data. However, this poses the problem of the influence of thermal fluctuations. These fluctuations have not been introduced in the model, but are expected to become important when the drop is elongated. Indeed, a thermal noise in the problem could reduce the restabilization processes, and reduce the data dispersion. This is of course a conjecture that needs to be further investigated.

ACKNOWLEDGMENT

The authors are grateful to the "Institut de Physique de la Matière Condensée" (IPMC) for a special grant devoted to computations.

[1] G. I. Taylor, Proc. R. Soc. London, Ser. A **138**, 41 (1932).
[2] G. I. Taylor, Proc. R. Soc. London, Ser. A **146**, 501 (1934).
[3] H. P. Grace, Chem. Eng. Commun. **14**, 225 (1982).
[4] B. J. Bentley and L. G. Leal, J. Fluid Mech. **167**, 241 (1986).
[5] S. Torza, R. G. Cox, and S. G. Mason, J. Colloid Interface Sci. **38**, 395 (1972).
[6] D. Barthès-Biesel and A. Acrivos, J. Fluid Mech. **61**, 1 (1973).
[7] J. D. Buckmaster, J. Fluid Mech. **55**, 385 (1972).
[8] E. J. Hinch and A. Acrivos, J. Fluid Mech. **91**, 401 (1979).
[9] A. Acrivos and T. S. Lo, J. Fluid Mech. **86**, 641 (1978).
[10] O. A. Ladyzhenskaya, *The Mathematical Theory of Viscous Incompressible Flow*, 2nd ed. (Gordon & Breach, London, 1969).
[11] J. M. Rallison and A. Acrivos, J. Fluid Mech. **89**, 191 (1978).
[12] H. A. Stone and L. G. Leal, J. Fluid Mech. **198**, 399 (1989).
[13] A. Z. Zinchenko, M. A. Rother, and R. H. Davis, Phys. Fluids **9**, 1493 (1997).
[14] C. Pozrikidis, *Boundary Integral and Singularity Methods for Linearized Viscous Flows* (Cambridge University Press, Cambridge, U.K., 1992).
[15] J. Eggers, Rev. Mod. Phys. **69**, 865 (1997).
[16] J. R. Lister and H. A. Stone, Phys. Fluids **10**, 2758 (1998).
[17] I. Cohen, M. P. Brenner, J. Eggers, and S. R. Nagel, Phys. Rev. Lett. **83**, 1147 (1999).
[18] D. R. Webster and E. K. Longmire, Exp. Fluids **30**, 47 (2001).
[19] Y. Y. Renardy and V. Cristini, Phys. Fluids **13**, 2161 (2001).
[20] S. Tomotika, Proc. R. Soc. London, Ser. A **150**, 322 (1935).
[21] S. Tomotika, Proc. R. Soc. London, Ser. A **153**, 302 (1936).
[22] M. Sussman, P. Smereka, and S. Osher, J. Comput. Phys. **114**, 146 (1994).
[23] M. Sussman, E. Fatemi, P. Smereka, and S. Osher, Comput. Fluids **27**, 663 (1998).
[24] S. B. Pillapakkam and P. Singh, J. Comput. Phys. **174**, 552 (2001).
[25] J. Li, Y. Y. Renardy, and M. Renardy, Phys. Fluids **12**, 269 (2000).
[26] J. Beaucourt, F. Rioual, T. Sèon, T. Biben, and C. Misbah, Phys. Rev. E **69**, 011906 (2004).
[27] T. Biben, C. Misbah, A. Leyrat, and C. Verdier, Europhys. Lett. **63**, 623 (2003).
[28] P. Yue, J. J. Feng, C. Liu, and J. Shen, J. Fluid Mech. **515**, 293 (2004).
[29] H. Haj-Hariri, Q. Shi, and A. Borhan, Phys. Fluids **6**, 2555 (1994).
[30] R. Chella and J. Vinals, Phys. Rev. E **53**, 3832 (1996).
[31] D. M. Anderson, G. B. McFadden, and A. A. Wheeler, Physica D **135**, 175 (2000).
[32] J. Li and Y. Y. Renardy, J. Non-Newtonian Fluid Mech. **95**, 235 (2000).
[33] Y. T. Hu, D. J. Pine, and L. G. Leal, Phys. Fluids **12**, 484 (2000).
[34] H. A. Stone and L. G. Leal, J. Fluid Mech. **220**, 161 (1990).
[35] D. Barthès-Biesel and H. Sgaier, J. Fluid Mech. **160**, 119 (1985).
[36] G. K. Batchelor, J. Fluid Mech. **41**, 545 (1970).
[37] N. A. Frankel and A. Acrivos, J. Fluid Mech. **44**, 65 (1970).
[38] K. M. B. Janssen, W. G. M. Agterof, and J. Mellema, J. Rheol. **45**, 227 (2001).
[39] D. C. Tretheway and L. G. Leal, J. Non-Newtonian Fluid Mech. **99**, 81 (2001).
[40] J.-W. Ha and L. G. Leal, Phys. Fluids **13**, 1568 (2001).
[41] J. S. Rowlinson and B. Widom, *Molecular Theory of Capillarity* (Oxford University Press, Oxford, 1989).
[42] J. W. Cahn and S. M. Allen, J. Phys. (Paris), Colloq. **38**, C7-51 (1977).
[43] S. M. Allen and J. W. Cahn, Acta Metall. **27**, 1085 (1979).
[44] D. Jasnow and J. Vinals, Phys. Fluids **8**, 660 (1996).
[45] R. Folch, J. Casademunt, A. Hernandez-Machado, and L. Ramirez-Piscina, Phys. Rev. E **60**, 1724 (1999).
[46] R. Almgren, J. Comput. Phys. **106**, 337 (1993).
[47] A. A. Wheeler, B. T. Murray, and R. J. Schaefer, Physica D **66**, 243 (1993).
[48] J. D. Buckmaster and J. E. Flaherty, J. Fluid Mech. **60**, 625 (1973).
[49] H. A. Stone, B. J. Bentley, and L. G. Leal, J. Fluid Mech. **173**, 131 (1986).
[50] H. A. Stone, Annu. Rev. Fluid Mech. **26**, 65 (1994).
[51] H. A. Stone and L. G. Leal, J. Fluid Mech. **206**, 223 (1989).